Quantum Thermal Bath for Path Integral Molecular Dynamics Simulation

Fabien Brieuc, Hichem Dammak, Marc Hayoun

▶ **To cite this version:**

Fabien Brieuc, Hichem Dammak, Marc Hayoun. Quantum Thermal Bath for Path Integral Molecular Dynamics Simulation. Journal of Chemical Theory and Computation, 2016, 12 (3), pp.1351 - 1359. 10.1021/acs.jctc.5b01146 . hal-01932606

HAL Id: hal-01932606

https://centralesupelec.hal.science/hal-01932606

Submitted on 23 Nov 2018

HAL is a multi-disciplinary open access archive for the deposit and dissemination of scientific research documents, whether they are published or not. The documents may come from teaching and research institutions in France or abroad, or from public or private research centers.

L'archive ouverte pluridisciplinaire **HAL**, est destinée au dépôt et à la diffusion de documents scientifiques de niveau recherche, publiés ou non, émanant des établissements d'enseignement et de recherche français ou étrangers, des laboratoires publics ou privés.

Quantum Thermal Bath for Path Integral Molecular Dynamics Simulation[†]

Fabien Brieuc,[‡] Hichem Dammak,[*,‡,¶] and Marc Hayoun[¶]

[‡]*Laboratoire Structures, Propriétés et Modélisation des Solides, CNRS, CentraleSupélec, Université Paris-Saclay, F-92295 Châtenay-Malabry, France*

[¶]*Laboratoire des Solides Irradiés, CNRS, CEA, École Polytechnique, Université Paris-Saclay, F-91128 Palaiseau, France*

E-mail: hichem.dammak@centralesupelec.fr

Abstract

The quantum thermal bath (QTB) method has been recently developed to account for the quantum nature of the nuclei by using standard molecular dynamics (MD) simulation. QTB-MD is an efficient but approximate method for dealing with strongly anharmonic systems, while path integral molecular dynamics (PIMD) gives exact results in a huge amount of computation time. The QTB and PIMD methods have been combined in order to improve the PIMD convergence or correct the failures of the QTB-MD technique. A new power spectral density of the random force within the QTB has therefore been developed. A modified centroid-virial estimator of the kinetic energy, especially adapted to QTB-PIMD, has also been proposed. The method is applied to selected systems: a one-dimensional double well system, a ferroelectric phase transition, and the position distribution of an hydrogen atom in a fuel cell material. The advantage of the QTB-PIMD method is its ability to give exact results with a more reasonable computation time for strongly anharmonic systems.

[†]J. Chem. Theory Comput. 12, (2016) 1351-1359. DOI: 10.1021/acs.jctc.5b01146

1 Introduction

[1] The quantum nature of nuclei can play a major role at low temperatures and/or in systems containing light atoms. In this case, nuclear quantum effects cannot be neglected and have to be taken into account in atomistic simulations. A standard way of including them is to use path integral methods[1–3] such as path integral molecular dynamics (PIMD) which provide exact quantum results even for strongly anharmonic systems. Unfortunately, time correlation functions are not accessible and require the use of techniques such as ring polymer molecular dynamics[4] or centroid molecular dynamics.[5] Moreover, the computation time required for PIMD reduces its range of applicability, in particular when using a first-principle description of the interatomic forces.

Alternative techniques based on a modified Langevin equation have recently been proposed to include nuclear quantum effects in molecular dynamics (MD) simulations.[6,7] Among them the quantum thermal bath (QTB) method[6] is an approximate approach, very simple to implement in an existing MD code, and that yields accurate results for various types of systems.[8–13] In addition, it requires the same amount of computation time as standard MD and time correlation functions are directly accessible. The QTB method becomes approximate when dealing with strongly anharmonic systems and therefore suffers from the zero-point energy (ZPE) leakage.[14,15] The ZPE leakage is a known problem[16–19] in classical trajectories where energy flows from the high-frequency modes, with large zero-point energies, to low-frequency modes with smaller zero-point energies. An empirical solution reducing the ZPE leakage within the QTB method has been attempted but with limited efficiency.[14,15]

In this work, the QTB is combined with the PIMD method in order (i) to avoid the ZPE leakage within QTB for strongly anharmonic systems and (ii) to reduce the computation time of PIMD. The convergence of the PIMD is significantly accelerated since less replicas are needed for convergence. The combination of QTB with PIMD is first described and then applied to selected systems: a one-dimensional double well system, a ferroelectric phase

[1] J. Chem. Theory Comput. 12, (2016) 1351-1359. DOI: 10.1021/acs.jctc.5b01146

transition, and the position distribution of an hydrogen atom in a fuel cell material.

2 Combining Path integrals with the quantum thermal bath

[2]The goal is to combine the PIMD with the QTB method in a way similar to that developed by Ceriotti *et al.*[20] In our case, the idea is to replace the classical thermostat applied to each bead of the polymer by the QTB. To achieve this, it is necessary to find the appropriate power spectral density of the random force which will then depend on the number of replicas, P.

2.1 Equations of dynamics

In both the PIMD and the combined QTB-PIMD formalisms, the equation of motion of each atom i ($i = 1, \cdots, N$) of a replica s ($s = 1, \cdots, P$) is given by

$$\dot{\mathbf{p}}_{i,s} = \frac{1}{P}\,\mathbf{f}_{i,s} - m_i\omega_P^2\,(2\mathbf{r}_{i,s} - \mathbf{r}_{i,s+1} - \mathbf{r}_{i,s-1}) - \gamma\,\mathbf{p}_{i,s} + \mathbf{R}_{i,s} \tag{1}$$

where $\mathbf{r}_{i,s}$, $\mathbf{p}_{i,s}$, and $\mathbf{f}_{i,s}$ are the atomic position, the momentum, and the force exerted by all the other atoms of the replica s. The spring constant between beads is equal to

$$m_i\omega_P^2 = \frac{m_i\,P\,k_B^2\,T^2}{\hbar^2} \tag{2}$$

The last two terms of eq 1 correspond to the friction and stochastic forces of the thermostat, respectively.

The power spectral density of the random force, I_{R_i}, is obtained from the fluctuation-

[2]J. Chem. Theory Comput. 12, (2016) 1351-1359. DOI: 10.1021/acs.jctc.5b01146

dissipation theorem:[21,22]

$$I_{R_i}(\omega, T) = 2\, m_i\, \gamma\, \kappa(\omega, T) \tag{3}$$

In standard PIMD, when the Langevin thermostat is used, the stochastic force is a white noise and $\kappa(\omega, T) = k_B\, T$. For the combined QTB-PIMD, the power spectral density is ω-dependent and corresponds to the energy of the oscillator ω, which matches the energy $\theta(\omega, T)$ of the quantum harmonic oscillator when $P = 1$. $\kappa(\omega, T)$ will be determined in section 2.2. The correlation function of the random force satisfies the Wiener-Khinchin theorem:

$$\langle R_{i,s,\alpha}(t) R_{i,s,\alpha}(t+\tau)\rangle = \int_{-\infty}^{+\infty} I_{R_i}(\omega, T)\ \exp[-i\omega\ \tau]\frac{d\omega}{2\pi} \tag{4}$$

The random force $R_{i,s,\alpha}(t)$ is computed using the numerical technique described in the Appendix of Ref.[23]

2.2 Derivation of the power spectral density

[3]Considering a one-dimensional (1D) harmonic potential energy: $V(x) = \frac{1}{2} m\omega^2\, x^2$, the quantum mean square fluctuation of the position x at temperature T is given by

$$\left\langle x^2 \right\rangle = \frac{1}{m\,\omega^2}\,\theta(\omega, T) = \frac{\hbar}{2\,m\,\omega}\coth\left(\beta\frac{\hbar\omega}{2}\right) \tag{5}$$

where $\beta = 1/(k_B T)$. In the PIMD scheme, one can transform the coordinates of the P replicas, $x_1, \cdots, x_s, \cdots, x_P$, into normal modes, $q_0, \cdots, q_k, \cdots, q_{P-1}$ with pulsations

$$\omega_k^2 = \frac{\omega^2}{P} + 4\,\omega_P^2 \sin^2\left(\frac{k\,\pi}{P}\right) \tag{6}$$

and the mean square fluctuation is then obtained according to

$$\left\langle x^2 \right\rangle = \frac{1}{P}\sum_{k=0}^{P-1}\left\langle q_k^2 \right\rangle \tag{7}$$

[3]J. Chem. Theory Comput. 12, (2016) 1351-1359. DOI: 10.1021/acs.jctc.5b01146

The mean potential energy of the normal modes is equal to $\frac{1}{2}\kappa(\omega_k, T)$ and then

$$\left\langle q_k^2 \right\rangle = \frac{1}{m\,\omega_k^2}\,\kappa(\omega_k, T) \tag{8}$$

Now, let us determine κ when performing QTB-PIMD. The function $\kappa(\omega, T)$ must allow one to recover the expected position fluctuation given by eq 5

$$\frac{1}{P}\sum_{k=0}^{P-1}\frac{1}{m\,\omega_k^2}\,\kappa(\omega_k, T) = \frac{\hbar}{2\,m\,\omega}\coth\left(\beta\frac{\hbar\omega}{2}\right) \tag{9}$$

Defining the dimensionless quantities

$$u = \beta\frac{\hbar\omega}{2} \tag{10}$$

$$h(u) = u\,\coth(u) \tag{11}$$

$$f_P^{(0)}(u) = \frac{\beta}{P}\,\kappa\left(\frac{2u}{\beta\,\hbar}\right) \tag{12}$$

eq 9 becomes

$$\sum_{k=0}^{P-1}\frac{u^2}{u_k^2}\,f_P^{(0)}(u_k) = h(u) \tag{13}$$

where u_k is the reduced pulsation according to equations 6 and 10

$$u_k^2 = \frac{u^2}{P} + P\,\sin^2\left(\frac{k\,\pi}{P}\right) \tag{14}$$

In the definition of κ through eq 9 all the normal modes are treated in the same way. There is an alternative definition[24] in which the normal mode at $k = 0$ (centroid of the ring polymer) is classically considered, i. e. $\kappa(\omega_0, T) = k_B T$. In this case, eq 9 becomes

$$\frac{1}{P}\frac{k_B\,T}{m\,\omega_0^2} + \frac{1}{P}\sum_{k=1}^{P-1}\frac{1}{m\,\omega_k^2}\,\kappa(\omega_k, T) = \frac{\hbar}{2\,m\,\omega}\coth\left(\beta\frac{\hbar\omega}{2}\right) \tag{15}$$

Using the same dimensionless quantities eq 15 leads to a new equation to be solved

$$\sum_{k=1}^{P-1} \frac{u^2}{u_k^2} f_P^{(1)}(u_k) = h(u) - 1 \tag{16}$$

Equations 13 and 16 can be solved by using the self-consistent iterative technique of Ceriotti *et al.*[20] The numerical calculation of $f_P^{(0)}$ [25] and $f_P^{(1)}$ are reported in Appendix A.

2.3 The estimation of macroscopic properties

[4]In the PIMD method, the potential energy, U, is calculated using the expression

$$U = \frac{1}{P} \sum_s V(\mathbf{r}_{1,s}, \cdots, \mathbf{r}_{N,s}) \tag{17}$$

whereas two expressions for the estimator of the kinetic energy are usually used; the primitive estimator given by

$$K_{prim} = \sum_{i,s} \frac{\mathbf{p}_{i,s}^2}{2\, m_i} - \sum_{i,s} \frac{1}{2} m_i \omega_P^2 (\mathbf{r}_{i,s} - \mathbf{r}_{i,s+1})^2 \tag{18}$$

and the centroid-virial estimator given by

$$K_{Cvir} = \frac{3N}{2} k_B T - \frac{1}{2P} \sum_{i,s} (\mathbf{r}_{i,s} - \mathbf{r}_i^c) \cdot \mathbf{f}_{i,s} \tag{19}$$

where $\mathbf{r}_i^c = \sum_s \mathbf{r}_{i,s}/P$ is the centroid of the ring polymer i. The last estimator is known to exhibit weaker fluctuations, which are insensitive to P compared to the primitive estimator for which fluctuations grow with P.[2] Combining the QTB and PIMD methods includes a part of the quantum fluctuations in the momenta, i.e.

$$\left\langle \sum_{i,s} \frac{\mathbf{p}_{i,s}^2}{2\, m_i} \right\rangle \; > \; \frac{3NPk_B T}{2} \tag{20}$$

[4]J. Chem. Theory Comput. 12, (2016) 1351-1359. DOI: 10.1021/acs.jctc.5b01146

thus expression 19 underestimates the kinetic energy for the QTB-PIMD method and it is more suitable to replace the classical energy $\frac{3}{2}Nk_BT$ by P times the kinetic energy of the N normal modes centroids as follows

$$K_{mCvir} = P\sum_i \frac{(\mathbf{p}_i^c)^2}{2m_i} - \frac{1}{2P}\sum_{i,s}(\mathbf{r}_{i,s} - \mathbf{r}_i^c)\cdot\mathbf{f}_{i,s} \tag{21}$$

where $\mathbf{p}_i^c$ is the momentum of the centroid i. The factor P takes into account the factor $\sqrt{P}$ between the centroid coordinate and the normal mode coordinate $\mathbf{q}_{i,0} = \sum_s \mathbf{r}_{i,s}/\sqrt{P}$ of the ring i.

The two expressions, 19 and 21, are equivalent for any interatomic potential in the case of the original PIMD, but only for harmonic potentials in the case of QTB-PIMD using the $f_P^{(1)}$ function. In the case of an anharmonic potential, each centroid i, i.e. the normal mode $\mathbf{q}_{i,0}$, is coupled to the other normal modes of the corresponding polymer. Consequently, the centroid temperature is different from the thermostat one (QTB), since a part of the quantum effects is included in the momenta of the internal modes $\mathbf{q}_{i,k>0}$ of the polymer. On the other hand, only expression 21 may be used for the QTB-PIMD using the $f_P^{(0)}$ function, because in this case the dynamics of the centroid also includes quantum effects.

Next, we want to compare the two formulations of the QTB-PIMD method using either the $f_P^{(0)}$ or $f_P^{(1)}$ functions (eq 13,16) and to choose the adequate kinetic energy estimator among expressions 18, 19, and 21. For this, let us consider a system for which the pressure is zero and thus the kinetic and potential contributions cancel each other out. This allows one to express the kinetic energy using the virial estimator,[26,27] K_{vir}, from the general expression of the pressure

$$p\,\mathcal{V} = \frac{2}{3}K + \frac{1}{3P}\left\langle \sum_{i,s}\mathbf{r}_{i,s}\cdot\mathbf{f}_{i,s}\right\rangle \tag{22}$$

$$K_{vir} = -\frac{1}{2P}\sum_{i,s}\mathbf{r}_{i,s}\cdot\mathbf{f}_{i,s} \tag{23}$$

This estimator is used as a reference to validate the relevance of the other estimators. The test is performed on two cases of the Morse potential characterized by the dimensionless parameter λ defined as

$$\frac{1}{\lambda^2} = \hbar^2\alpha^2/(2mD) \tag{24}$$

where D and α^{-1} are the depth and width of the well, and m is the reduced mass. The anharmonicity of the potential can be expressed as the relative shift of the ground state energy with respect to the harmonic approximation value, $(4\lambda^2)^{-1}$. The first case is weakly anharmonic ($\lambda^{-2} = 0.0015$ as the case of the HCl molecule) while for the second case the anharmonicity is chosen to be more important ($1/\lambda^2 = 0.024$).

Figure 1 shows that the QTB-PIMD method, either using $f_P^{(0)}$ or $f_P^{(1)}$, allows a faster convergence with the number of beads than the PIMD one, as expected. For both methods the convergence is slower in the case of the more anharmonic potential. For the weakly anharmonic model, the potential energy (Figure 1(a)) remains almost constant as a function of P showing that the QTB approach ($P = 1$) already provides a value very close to the exact one. The kinetic energy behaves similarly (Figure 1(b)) but depends on the estimator. For the two potential models, it is worth noting that K_{prim} and K_{Cvir} systematically give the highest and the lowest values for the kinetic energy, respectively (Figures 1(b) and 1(d)). In contrast, K_{mCvir} provides values very close to those obtained with K_{vir} which is considered as a reference in this example. Figure 2 shows the influence of the effective friction coefficient γ on the kinetic energy estimators. It is clearly shown that K_{mCvir} (eq 21) provides the better estimation and is, in particular, insensitive to γ when using the $f_P^{(1)}$ function, whereas the primitive estimator needs the use of a low value of γ leading to the increase of the computation time.

This example shows that both definitions of the f_P functions (eq 13 and eq 16) allow similar convergences of the potential and kinetic energies with the number of beads. The best estimator for the kinetic energy is the modified centroid-virial one given by eq 21. In the following sections it is also shown that position distributions of atoms obtained by using

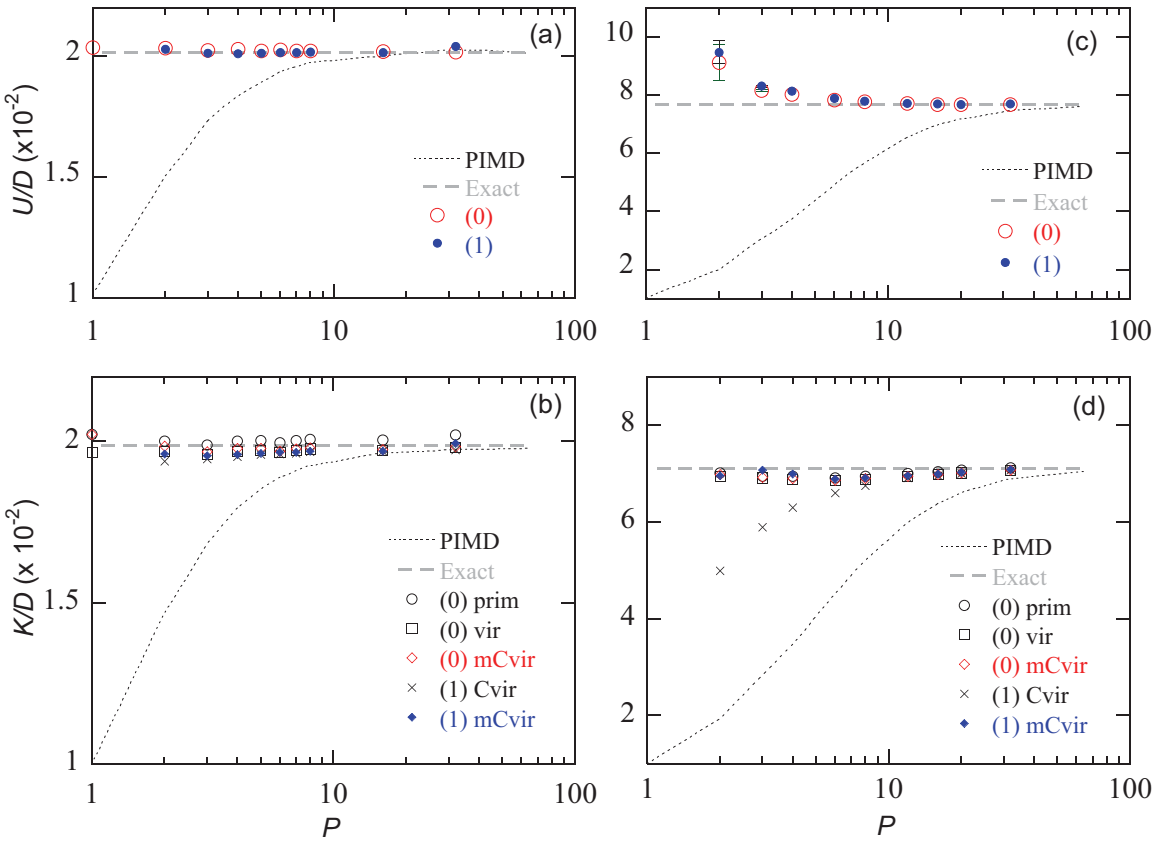

Figure 1: Convergence of the potential, U, and kinetic, K, energies as a function of the bead number for PIMD and QTB-PIMD simulations using either $f_P^{(0)}$ or $f_P^{(1)}$, herein referenced as (0) and (1), respectively. Case of two Morse potentials, $\lambda^{-2} = 0.00145$ for (a) and (b), and $\lambda^{-2} = 0.024$ for (c) and (d). The energies are normalized by the well depth, D, and calculations were carried out at $T = 0.02\, D/k_B$. K values were obtained using either primitive (prim), virial (vir), centroid-virial (Cvir) or modified centroid-virial (mCvir) estimators given by equations 18, 23, 19 and 21, respectively. The exact values were derived by numerically solving the Schrödinger equation and occupying the resulting eigenstates with the proper Boltzmann factor.

$f_P^{(0)}$ or $f_P^{(1)}$ are very close.

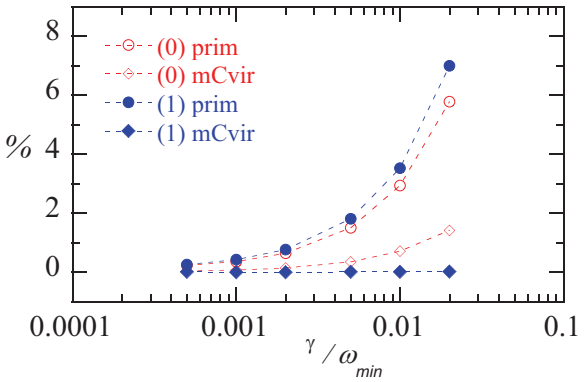

Figure 2: Effect of the effective friction coefficient γ on the kinetic energy obtained by using the primitive (prim) and modified centroid-virial (mCvir) estimators. (0) and (1) correspond to QTB-PIMD simulations using $f_P^{(0)}$ and $f_P^{(1)}$ functions respectively. The relative deviation from the virial estimator values, $(K-K_{vir})/K_{vir}$, is plotted. γ is normalized by the pulsation ω_{min} which is equal to that of the centroid (normal mode $k=0$ of the ring polymer) in the harmonic approximation: $\omega_{min} = \omega_0 = \omega/\sqrt{P}$ (eq 6) . Case of the Morse potential where $1/\lambda^2 = 0.00145$ using $P=4$ and $T = 0.02\, D/k_B$.

3 Applications

3.1 Position distribution in a one-dimensional double well potential

[5]Let us consider a particle of mass m in a double well potential

$$V(x) = V_0 \left[(x/a)^2 - 1\right]^2 \tag{25}$$

Using reduced units

$$y = x/a, \epsilon = E/V_0 \tag{26}$$

for the position and the energy respectively, the equation for the stationary wave functions ϕ writes

$$-C\,\frac{d^2\phi}{dy^2} + (y^2-1)^2\,\phi = \epsilon\,\phi \tag{27}$$

[5]J. Chem. Theory Comput. 12, (2016) 1351-1359. DOI: 10.1021/acs.jctc.5b01146

where C is a parameter depending on the barrier height, V_0, and the distance between the two wells, $2a$

$$C = \hbar^2/(2ma^2V_0) \tag{28}$$

The numerical resolution of eq 27 shows that there exists a critical value for the parameter, $C_0 = 0.731778$, when the ground state energy equals V_0. The eigenvalues rely on C and we find in particular that the energy of the ground state, ϵ_0, is lower than the height of the energy barrier, i. e. $\epsilon_0 < 1$, when $C < C_0$. The motivation behind using such a one-dimensional quartic double-well potential is to provide a simple model to check the ability of the QTB-PIMD method to recover the tunnel effect in contrast to the original QTB approach.[28,29] We investigate the position distribution of a particle in this double-well potential at a reduced temperature $T^* = k_B\,T/\epsilon_0 = 0.4$ for three values of the C parameter: 1, 0.3, and 0.1.

The position probability density, $\rho(y)$, obtained by QTB-PIMD simulation is compared to the exact one, $\rho_0(y)$, obtained by numerically solving the Schrödinger equation and occupying the resulting eigenstates with the proper Boltzmann factor. The convergence of the density is evaluated by calculating the divergence factor d_P

$$d_P = \sqrt{\frac{\int_{-\infty}^{+\infty}(\rho - \rho_0)^2\,dy}{\int_{-\infty}^{+\infty}\rho_0^2\,dy}} \tag{29}$$

similar to the reliability factor used in the Rietveld method[30] to refine a theoretical line profile until it matches an experimental profile.

In all cases, the evolution of the divergence factor and the distributions as a function of P obtained with the QTB-PIMD method are similar when using either the $f_P^{(0)}$ or the $f_P^{(1)}$ function.

Figure 3 shows the evolution of the divergence factor as a function of the number of beads for the three investigated cases. In the first case, the value of the C parameter , $C = 1$, is greater than the critical value C_0 (eq 28). As shown by the divergence factor in Figure 3(a), the distributions obtained with the QTB-PIMD and PIMD methods converge to the exact

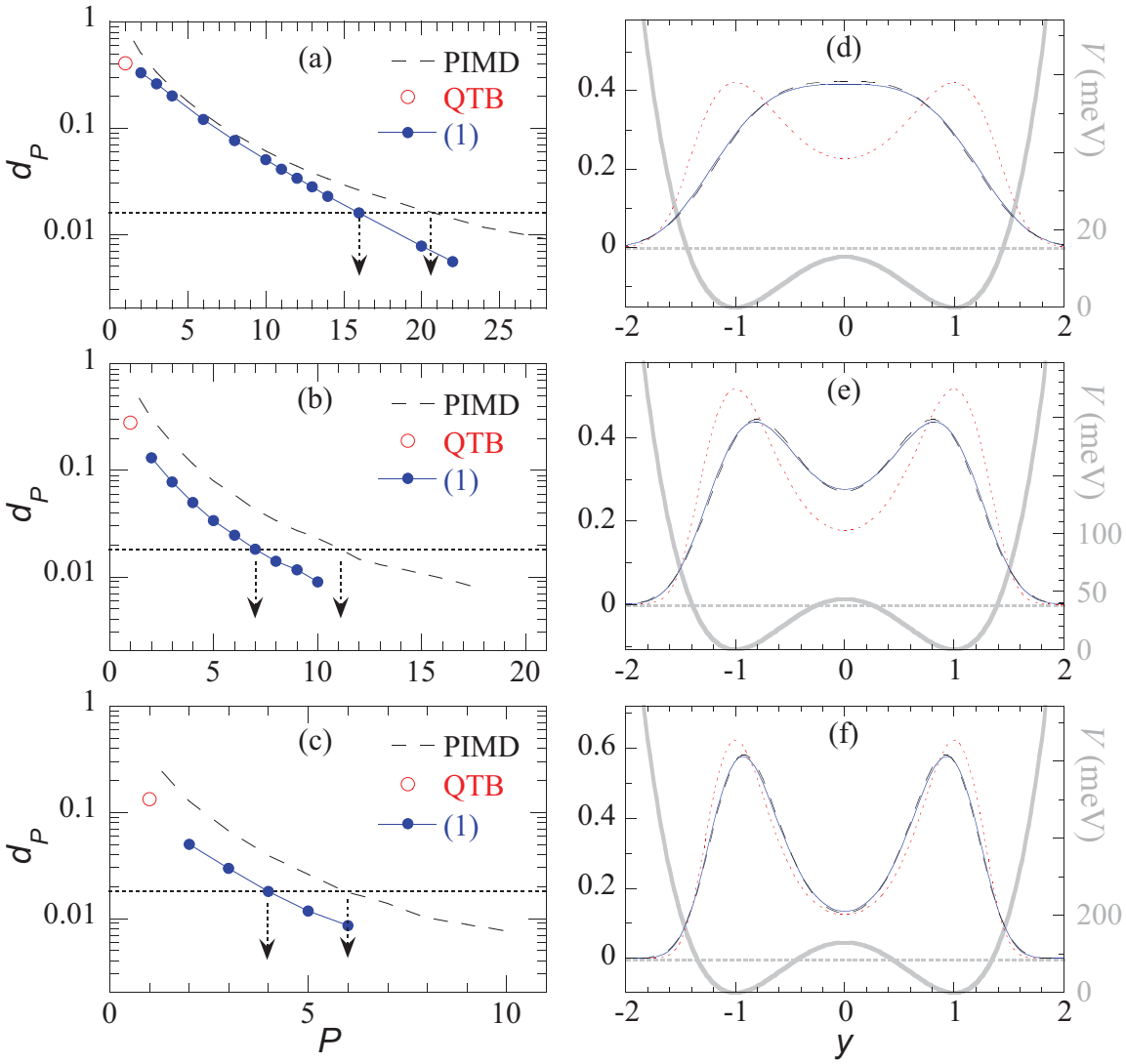

Figure 3: Divergence factor, d_P, as a function of the number of beads for the double-well potential given by eq 27. Three cases of this potential are investigated: (a) $C = 1.0$, (b) $C = 0.3$, and (c) $C = 0.1$. Calculations have been carried out at a reduced temperature T^* of 0.4 for PIMD, QTB, and QTB-PIMD using the $f_P^{(1)}$ function. The arrows indicate the smallest numbers of beads obtained for $d_P < 2\%$. The calculated position distributions corresponding to the QTB-PIMD case are shown (full line) in (d) $P = 16$, (e) $P = 7$, and (f) $P = 4$, together with the exact solution (dashed line). The QTB position distribution is also plotted (dotted line) for comparison purposes. The potential energy curves are superimposed (gray full line) and the horizontal gray dotted lines show the total energy of the system in each case; the values of the barrier height V_0 are deduced from C through eq 28 for the hydrogen atom and the distance between minima is fixed at $2a = 0.8$ Å.

one, within an error of about $d_P = 2\%$ at $P = 16$ and $P = 21$, respectively. Hence, the full convergence is especially difficult to reach in this case. Indeed, the exact distribution

exhibits only one maximum located at $y = 0$ (Figure 3(d)), while a poor convergence leads to a distribution with two maxima. One of these situations is illustrated by the QTB method which dramatically fails with an error of $d_P = 40\%$. In the two other cases, C is lower than C_0 and all the position distributions show two maxima (Figures 3(e) and 3(f)). For the QTB-PIMD simulation, the number of beads required to converge whithin an error of about $d_P = 2\%$ decreases when C decreases; P equals 7, and 4 for $C = 0.3$, and $C = 0.1$, respectively (Figures 3(b) and 3(c)). It is worth noting that, for the lowest value of C, the distribution obtained with the QTB method is in good agreement with the exact one. This case corresponds to high values of either the barrier height, V_0, or the distance, $2a$, between the two wells, or the particle mass, m. In other words, the QTB method succeeds when the tunnel effect is not predominant.

In summary, the combination of the QTB and the PIMD methods allows a better convergence with the number of beads. In fact, for a high accuracy in the position distribution the gain obtained by QTB-PIMD with respect to PIMD is not so important and is lower than a factor of two. In contrast, the advantage of the QTB-PIMD is more substantial – a gain of a factor of three – with respect to the convergence of the total energy.

3.2 Ferroelectric-paraelectric phase transition

[6]We now investigate the $BaTiO_3$ (BTO) ferroelectric crystal which is characterized by a complex multiple-well energy landscape affecting the polar degrees of freedom. In this compound the quantum effects significantly decrease the phase transition temperatures by $\approx$ 30-50 K[31] and strongly modify the shape of the pressure-temperature phase diagram[32] even at room temperature.

The ferroelectric properties of BTO are modeled by using the effective hamiltonian of Zhong *et al.*,[33] which was derived from first-principles density-functional calculations. This approach yields an excellent description of its complex sequence of phase transitions: rhom-

[6]J. Chem. Theory Comput. 12, (2016) 1351-1359. DOI: 10.1021/acs.jctc.5b01146

bohedral(R) - orthorhombic (O) - tetragonal (T) - cubic (C). The T-C phase transition temperature, T_C, is shifted from 300 K to 260 K when using the standard MD and PIMD methods, respectively.[34]

In this work, we investigate the convergence of the value of the phase transition temperature (T_C) as a function of the number of beads by performing either QTB-PIMD or PIMD simulation in the isothermal-isobaric ensemble.

Figure 4 displays the polarization as a function of the temperature obtained by QTB-PIMD compared to the converged PIMD result. Favorably, the QTB-PIMD method with a number of beads equal to 2 gives a transition temperature $T_C = 257$ K very close to that obtained by PIMD with $P = 16$ (259 K). In addition, the inset in Figure 4 shows that the convergence of the polarization of the ferroelectric phase is faster when using the $f_P^{(1)}$ function within the QTB-PIMD method. In contrast, the use of the QTB method (QTB-PIMD with $P = 1$) strongly underestimates the value of T_C by ~ 55 K. It is worth noting that the error of the QTB method is fixed solely by two replicas when combining QTB with PIMD. This means that the effects of the zero-point energy leakage associated to the use of the QTB have been suppressed by the combination.

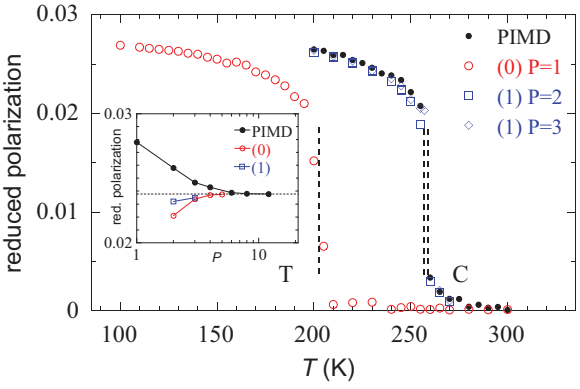

Figure 4: Temperature evolution of the reduced polarization associated to the tetragonal (T) to cubic (C) ferroelectric transition as obtained by PIMD ($P = 16$) and QTB-PIMD simulations using either $f_P^{(0)}$ or $f_P^{(1)}$ referenced as (0) and (1), respectively. Vertical dashed lines show the quick convergence of the Curie temperature obtained by QTB-PIMD: 202 K ($P = 1$), 257 K ($P = 2$), and 259 K ($P = 3$). The inset provides the convergence of the polarization at $T = 240$ K with the number of beads for the three methods.

3.3 Proton disorder in a fuel-cell oxide $BaZrO_3$

[7]We now investigate the proton disorder in the cubic phase of $BaZrO_3$ (BZO).[35,36] Indeed, it has been shown that perovskite type oxides (ABO_3) can exhibit high protonic conductivity[37] and that quantum effects play an important role. Among these oxides, doped BZO exhibits one of the highest conductivity combined with a good chemical stability[37,38] which makes it a potential candidate as electrolyte materials for proton conducting fuel cells.

The long range migration of a proton in a BZO crystal is a combination of transfer and reorientation mechanisms. During the transfer step the hydrogen atom jumps between the two neighboring oxygen atoms while, during the reorientation stage the hydrogen atom performs a rotation around the nearest oxygen atom. There are two possible rotations: one around the Zr-O-Zr axis and one around an axis orthogonal to the Zr-O-Zr axis with the hydrogen atom remaining in the same O-Zr-O plane.

The interactions between the atoms are modeled by an *ab initio* based force field[39] that reproduces the *ab initio* computed activation energies for the transfer and reorientation mechanisms.[39,40] The reactivity of the proton is included through the empirical valence bond model. No dopant is included in our simulations, so the distributions presented here illustrate the situation in a region far from the dopant atom. To ensure the electrical neutrality in the computations, a compensating uniform background charge is added. The MD simulations were performed within the canonical ensemble on a $3 \times 3 \times 3$ simulation box containing 136 atoms.

The 3D position distribution of one proton in BZO is computed at $T = 300$ K using QTB-PIMD and PIMD. As an illustration, the classical MD proton position distribution in the O-Zr-O plane is displayed in the top part of Figure 5. From this distribution one can note that the hydrogen atom remains bonded to the same oxygen atom, most of the time. One type of reorientation is essentially seen where the hydrogen atom performs a rotation around the nearest oxygen atom and remains in the same O-Zr-O plane. Figure 5 shows the

[7]J. Chem. Theory Comput. 12, (2016) 1351-1359. DOI: 10.1021/acs.jctc.5b01146

evolution of the position distribution with the number of beads as obtained by QTB-PIMD and PIMD. Quantum effects are important at this temperature since the classical distribution corresponding to PIMD with $P = 1$ is clearly different from the quantum distribution obtained by PIMD or QTB-PIMD with high P values. In the classical case the distribution exhibits two peaks, whereas in the quantum case the proton freely rotates around the nearest oxygen atom. Anyway, the transfer mechanism is rarely observed at $T = 300$ K. For the QTB-PIMD simulation, Figure 5 shows that the two peaks disappear from $P = 3$, and that the position distribution already converges to the exact one for $P = 4$. In contrast, the PIMD method requires a value of at least $P = 8$ for convergence. A more accurate comparison of the two methods is given in Figure 6 in which the corresponding divergence factors d_P (a generalization of eq 29 to 3D distributions) are plotted as a function of P. The PIMD calculations are converged within an error of $d_P = 8\%$ for $P = 6$, while the QTB-PIMD method requires a smaller number of beads, $P = 4$. We conclude as expected that QTB-PIMD is more efficient than the standard PIMD, since less replicas are needed for convergence.

4 Conclusion

[8]We have combined the path integral MD (PIMD) method with the quantum thermal bath (QTB) approach. This combination can be seen in two ways. In the first one, the QTB is used as a thermostat applied to standard PIMD in order to improve the PIMD convergence. Compared to standard PIMD this combination needs less replicas to converge – the gain is a factor of two or three – since a part of the quantum effects is included directly in the dynamics of the beads through the QTB. In the second way, a small number of replicas of the path integral allows the correction of the failures of the QTB-MD. Indeed, the QTB-MD technique gives rather satisfactory macroscopic properties for weakly anharmonic systems, especially away from phase transitions and in the case of non predominant tunnel effects. Thus, QTB-

[8]J. Chem. Theory Comput. 12, (2016) 1351-1359. DOI: 10.1021/acs.jctc.5b01146

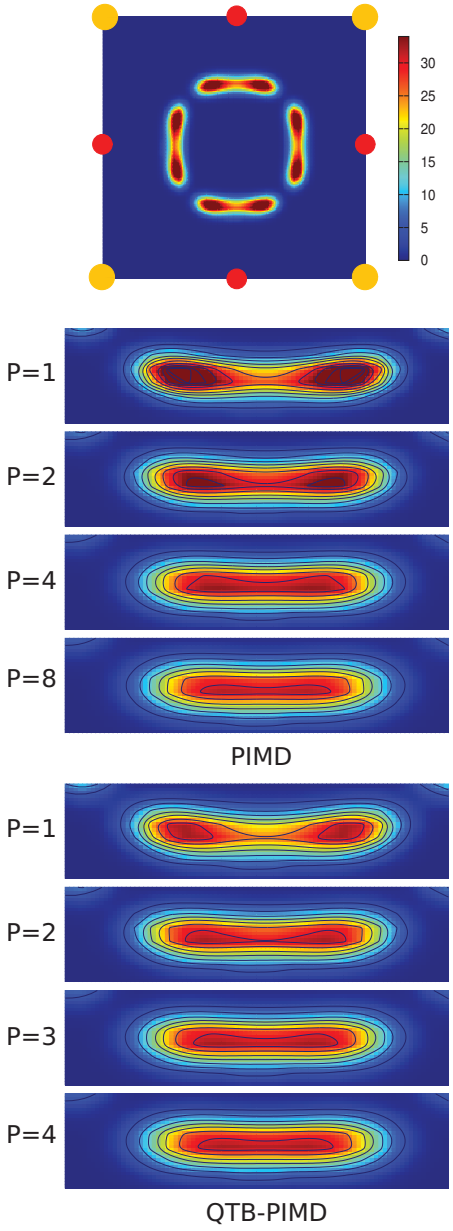

Figure 5: Position distribution of the proton in the O-Zr-O plane at $T = 300$ K as obtained by PIMD and QTB-PIMD simulations. The top image displays an example of the distribution in the unit cell (PIMD with $P = 1$) where one can distinguish the eight equivalent positions for the proton. The oxygen and zirconium atoms are shown by red and yellow full circles, respectively. The other images are enlargements of the distribution including contour lines to bring out the increase of the proton disorder by rotation around the neighbor oxygen atom as the number of beads increases.

MD stays an alternative method for who is not interested in high accuracy computations.

Small failures of the QTB can be fixed by only two replicas in QTB-PIMD. In contrast,

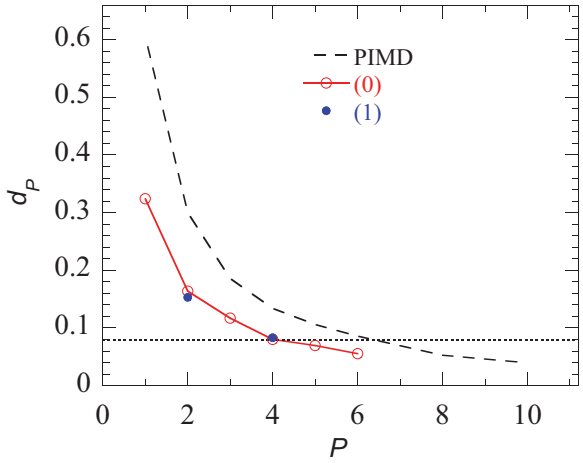

Figure 6: Divergence factor, d_P, (generalisation of eq 29 in 3D) as a function of the number of beads for the proton distribution in BZO at $T = 300$ K obtained by PIMD and QTB-PIMD simulations using either $f_P^{(0)}$ or $f_P^{(1)}$, herein referenced as (0) and (1), respectively. The horizontal dotted line allows one to determine the number of beads corresponding to $d_P = 0.08$.

when QTB-MD dramatically fails, QTB-PIMD can address the problem at the price of high computation cost. The advantage of the QTB-PIMD method is its ability to give exact results with a more reasonable computation time for strongly anharmonic systems including the tunnel effect between two wells. Unfortunately, as in PIMD, the major drawback of the new method is that the time dependent correlation functions are not directly accessible.

The combination with PIMD requires the modification of the power spectral density of the random force within the QTB. This spectral density is proportional to a reduced function (f_P) which can be defined in two ways. In the first one, random forces are applied to each bead of the ring polymer ($f_P^{(0)}$). An alternative way is to apply random forces to the normal modes of the ring polymer ($f_P^{(1)}$) except for the centroid mode dealt with a Langevin thermostat. It is shown that the $f_P^{(1)}$ function gives a better convergence of the macroscopic quantities with the number of beads than $f_P^{(0)}$. Considering that a part of the quantum fluctuations is included in the momenta through the QTB contribution, a modified centroid-virial estimator of the kinetic energy is proposed. This estimator is accurate and insensitive to the effective friction coefficient when using the $f_P^{(1)}$ function.

The combination procedure is similar to the one presented by Ceriotti *et al.*[20] The iterative algorithm described in Appendix A to determine the f_P function is the same as the one used to establish the g_P function of Ref. 20. The difference lies in the choice of the thermostat used to include the quantum effects. In the colored-noise thermostat (GLE) of Ceriotti *et al.*,[7] the quantum effects are introduced through a dispersive friction coefficient while in the QTB case the quantum effects are included through the power spectral density of the random force. The two methods are basically equivalent but the QTB-MD method is easier to implement in a PIMD code. Knowing the f_P function, the random forces can be directly generated.[23] In contrast, the GLE method requires to carefully optimize different parameters in the equations of motion (see eq. 8 of Ref. 20) in order to recover the quantum fluctuations.

The modified QTB is easy to include in any PIMD code and the implementation does not increase its complexity. The combination of the QTB and the PIMD methods within first principle descriptions is even more interesting. Such an implementation in the ABINIT code[41,42] is in progress. Moreover, the possibility of combining the modified QTB with methods such as ring polymer molecular dynamics (RPMD)[4] or centroid molecular dynamics (CMD)[5] will allow one to go beyond PIMD. In this case, time dependent correlation functions could be computed. Since the combination with the QTB consists in replacing the classical thermostat by the quantum thermal bath, the combination with RPMD (thermostated RPMD has been recently proposed[43]) or CMD would have the same complexity as the one of the QTB-PIMD. Let us point out that the combination requires the use of physical bead masses instead of fictitious ones.

A Self-consistent resolution of equations 13 and 16

[9]The $f_P^{(0)}$ and $f_P^{(1)}$ functions are determined through a self-consistent resolution of the equations.

[9]J. Chem. Theory Comput. 12, (2016) 1351-1359. DOI: 10.1021/acs.jctc.5b01146

In the case of the $f_P^{(0)}$ function, eq 13 can be reformulated by isolating the $k = 0$ term for which

$$u_0 = \frac{u}{\sqrt{P}} \tag{30}$$

$$f_P(\frac{u}{\sqrt{P}}) = \frac{1}{P}\left[h(u) - \sum_{k=1}^{P-1} \frac{f_P(u_k)}{(u_k^2/u^2)}\right] \tag{31}$$

The superscripts (0) is omitted for simplicity. Before solving, eq 31 is rewritten using the function

$$F_P(u) = f_p(u/\sqrt{P}) \tag{32}$$

$$F_P(u) = \frac{1}{P}\left[h(u) - \sum_{k=1}^{P-1} \frac{F_P(u_k\sqrt{P})}{(u_k^2/u^2)}\right] \tag{33}$$

We choose an initial solution with a good asymptotic behavior for eq 31:

$$F_P^{(0)}(u) = \frac{1}{P}h(u/P) \tag{34}$$

which matches the exact solution in the case $P = 1$. Using this initial solution and following Ceriotti *et al.*[20] the equation is iteratively solved as

$$F_P^{(i+1)}(u) = \frac{\alpha}{P}\left[h(u) - \sum_{k=1}^{P-1} \frac{F_P^{(i)}(u_k\sqrt{P})}{(u_k^2/u^2)}\right] + (1-\alpha)F_P^{(i)}(u) \tag{35}$$

where α is a weighting parameter whose value giving the best convergence is close to $1/P$. The random force of the QTB is generated from the power spectral density in the pulsation space in a range $[\omega_{min}; \omega_{max}]$. ω_{max} and ω_{min} are related to the MD time step δt and the time-length of a MD trajectory, respectively. It results in the $F_P(u)$ function needing to be determined in the correlated range $[u_{min}; u_{max}]$. Unfortunately, eq 35 shows that F_P must be calculated for the value $u_k\sqrt{P}$ which reaches a value, $\sqrt{u_{max}^2 + P^2}$, greater than u_{max}. To overcome this problem, the values of F_P for u greater than u_{max} are linearly extrapolated from the last 20% of the u range. The F_P function is obtained with enough accuracy over

about 30 iterations in eq 35. Results show that the function $f_P(u) = F_P(u\sqrt{P})$, directly related to the spectral energy $\kappa(\omega, T)$, tends to $1/P$ and $u/(P\sqrt{P})$ when u tends to 0 and ∞, respectively. Figure 7 presents the curves of the $f_P(u)$ solutions obtained for different values of P.

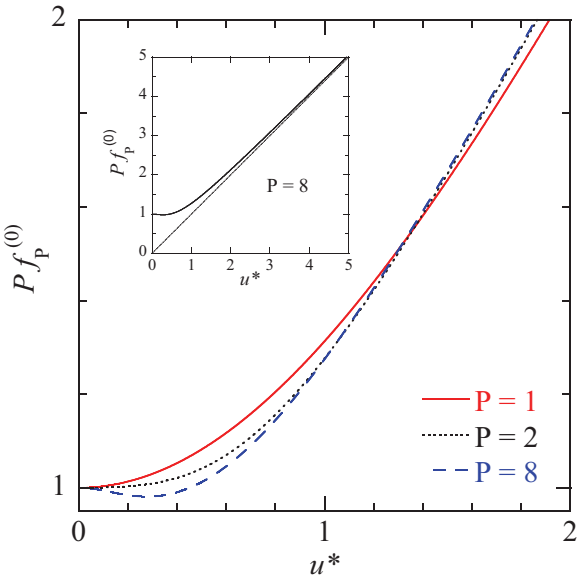

Figure 7: The $f_P^{(0)}$ function for different numbers of beads, P, as a function of $u^* = u/P\sqrt{P}$. The inset shows the asymptotic behavior at large values of u^*.

Now, let us consider the case of the $f_P^{(1)}$ function. Equation 16 can be reformulated by isolating the $k = 1$ term for which

$$u_1^2 = \frac{u^2}{P} + P\sin^2(\pi/P) \tag{36}$$

$$\frac{u^2}{u_1^2} f_P(u_1) = \left[h(u) - 1 - \sum_{k=2}^{P-1} \frac{f_P(u_k)}{(u_k^2/u^2)} \right] \tag{37}$$

The superscripts (1) is omitted for simplicity. Before solving, eq 37 is rewritten using the function

$$F_P(u) = f_p(u_1) \tag{38}$$

$$F_P(u) = \frac{u_1^2}{u^2} \left[h(u) - 1 - \sum_{k=2}^{P-1} \frac{u^2}{u_k^2} F_P\left(\sqrt{P u_k^2 - P^2 \sin^2(\pi/P)} \right) \right] \tag{39}$$

We choose an initial solution with a good asymptotic behavior for eq 37:

$$F_P^{(0)}(u) = \frac{1}{P-1}\left[h(u/P) - \frac{1}{P}\right]. \tag{40}$$

Using this initial solution, the equation is iteratively solved as

$$F_P^{(i+1)}(u) = \alpha\frac{u_1^2}{u^2}\left[h(u) - 1 - \sum_{k=2}^{P-1}\frac{u^2}{u_k^2}F_P\left(\sqrt{Pu_k^2 - P^2\sin^2(\pi/P)}\right)\right] + (1-\alpha)F_P^{(i)}(u) \tag{41}$$

where α is a weighting parameter whose value giving the best convergence is close to $1/P$. The $F_P(u)$ function is determined following the above mentioned procedure. Results show that the function

$$f_P(u) = F_P\left(\sqrt{Pu^2 - P^2\sin^2(\pi/P)}\right) \tag{42}$$

directly related to the spectral energy $\kappa(\omega, T)$, tends to $u/((P-1)\sqrt{P})$ when u tends to ∞. Figure 8 presents the curves of the $f_P(u)$ solutions obtained for different values of P.

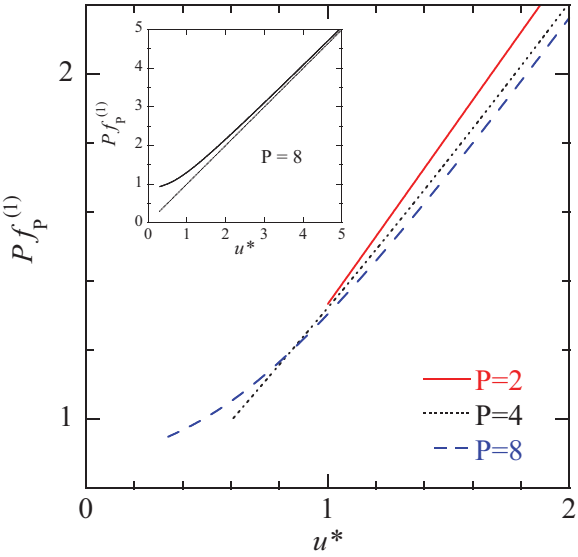

Figure 8: The $f_P^{(1)}$ function for different numbers of beads, P, as a function of $u^* = (\sqrt{P}\,u - 1)/(P-1)$. The inset shows the asymptotic behavior at large values of u^*.

Finally, the power spectral density thus obtained (eq 3, 10 and 12) through the $f_P^{(0)}$ or

$f_P^{(1)}$ functions

$$I_{R_i} = 2m_i\gamma\frac{P}{\beta}f_P(\beta\hbar\omega/2) \tag{43}$$

corresponds to that of the random forces $R_{i,k,\alpha}$ to be applied to normal modes (i,k) of the ring polymer (i). In the case of the $f_P^{(0)}$ function, one can show that the power spectral densities of the random forces applied to beads or to normal modes are equal. Hence, the random forces $R_{i,s,\alpha}$ can be directly generated according to eq 4. In contrast, for the $f_P^{(1)}$ function, since the centroid mode $(k = 0)$ is not dealt in the same way as the other normal modes $(k > 0)$, one has to first generate the random forces $R_{i,k,\alpha}$ and then to transform them into $R_{i,s,\alpha}$ by using the orthogonal transformation matrix C_{sk}

$$R_{i,s,\alpha} = \sum_k C_{sk}R_{i,k,\alpha} \tag{44}$$

$$C_{sk} = \begin{cases} \sqrt{1/P} & k = 0 \\ \sqrt{2/P}\cos(2\pi\, sk/P) & 0 < k < P/2 \\ \sqrt{1/P}(-1)^s & k = P/2 \\ \sqrt{2/P}\sin(2\pi\, sk/P) & P/2 < k < P \end{cases} \tag{45}$$

Acknowledgement

[10]This work was performed using HPC resources from the "mesocentre" computing center of CentraleSupélec, which is supported by CentraleSupélec and CNRS.

[10]J. Chem. Theory Comput. 12, (2016) 1351-1359. DOI: 10.1021/acs.jctc.5b01146

[11]

References

(1) Ceperley, D. M. *Rev. Mod. Phys.* **1995**, *67*, 279-355.

(2) Tuckerman, M. E. In *Statistical Mechanics: Theory and Molecular Simulation*; Ed.; Oxford University Press; New York, 2010, Chapter 12, pp 475-490.

(3) Marx, D.; Tuckerman, M. E.; Hutter, J.; Parrinello, M. *Nature* **1999**, *397*, 601-604.

(4) Craig, I. R.; Manolopoulos, D. E. *J. Chem. Phys* **2004**, *121*, 3368-3373.

(5) Cao, J.; Voth, G. A. *J. Chem. Phys.* **1994**, *100*, 5106-5117.

(6) Dammak, H.; Chalopin, Y.; Laroche, M.; Hayoun, M.; Greffet, J. J. *Phys. Rev. Lett.* **2009**, *103*, 190601.

(7) Ceriotti, M.; Bussi, G.; Parrinello, M. *Phys. Rev. Lett.* **2009**, *103*, 030603.

(8) Dammak, H.; Antoshchenkova, E.; Hayoun, M.; Finocchi, F. *J. Phys.: Condens. Matter* **2012**, *24*, 435402.

(9) Calvo, F.; Van-Oanh, N.; Parneix, P.; Falvo, C. *Phys. Chem. Chem. Phys.* **2012**, *14*, 10503-10506.

(10) Calvo, F.; Naumkin, F. Y.; Wales, D. J. *Chem. Phys. Lett.* **2012**, *551*, 38-41.

(11) Qi, T.; Reed, E. J. *J. Phys. Chem. A* **2012**, *116*, 10451-10459.

(12) Basire, M.; Borgis, D.; Vuilleumier, R. *Phys. Chem. Chem. Phys.* **2013**, *15*, 12591-12601.

(13) Bronstein, Y.; Depondt, P.; Finocchi, F.; Saitta, A. M. *Phys. Rev. B* **2014**, *84*, 214101.

[11] J. Chem. Theory Comput. 12, (2016) 1351-1359. DOI: 10.1021/acs.jctc.5b01146

(14) Bedoya-Martínez, O. N.; Barrat, J. L.; Rodney, D. *Phys. Rev. B* **2014**, *89*, 014303.

(15) Hernández-Rojas, J.; Calvo, F.; Noya, E. G. *J. Chem. Theory Comput.* **2015**, *11*, 861-870.

(16) Lu, D. H.; Hase, W. L. *J. Chem. Phys.* **1988**, *89*, 6723-6735.

(17) Miller, W. H.; Hase, W. L.; Darling, C. L. *J. Chem. Phys.* **1989**, *91*, 2863-2868.

(18) Bowman, J. M.; Gazdy, B.; Sun, Q. *J. Chem. Phys.* **1989**, *91*, 2859-2862.

(19) Habershon, S.; Manolopoulos, D. E. *J. Chem. Phys.* **2009**, *131*, 244518.

(20) Ceriotti, M.; Manolopoulos, D. E.; Parrinello, M. *J. Chem. Phys.* **2011**, *134*, 084104.

(21) Callen, H. B.; Welton, T. A. *Phys. Rev.* **1951**, *83*, 34-40.

(22) Kubo, R. *Rep. Prog. Phys.* **1966**, *29*, 255-284.

(23) Chalopin, Y.; Dammak, H.; Laroche, M.; Hayoun, M.; Greffet, J. J. *Phys. Rev. B* **2011**, *84*, 224301.

(24) Ceriotti, M.; Manolopoulos, D. E. *Phys. Rev. Lett.* **2012**, *109*, 100604.

(25) The f_P function is different from the g_P function of Ceriotti *et al.*[20] because the authors used another formulation of the PIMD (at temperature $P \times T$). Indeed, $f_P(u) = \frac{1}{P}\, g_P(u\sqrt{P})$.

(26) Herman, M. F.; Bruskin, E. J.; Berne, B. J. *J. Chem. Phys.* **1982**, *76*, 5150-5155.

(27) Parrinello, M.; Rahman, A. *J. Chem. Phys.* **1984**, *8*, 860-867.

(28) Barrozo, A. H.; de Koning, M. *Phys. Rev. Lett.* **2011**, *107*, 198901.

(29) Dammak, H.; Hayoun, M.; Chalopin, Y.; Greffet, J. J. *Phys. Rev. Lett.* **2011**, *107*, 198902.

(30) In *The Rietveld Method*; Young, R. A., Ed.; Oxford University Press, 1993.

(31) Zhong, W.; Vanderbilt, D. *Phys. Rev. B* **1996**, *53*, 5047-5050.

(32) Iniguez, J.; Vanderbilt, D. *Phys. Rev. Lett.* **2002**, *89*, 115503.

(33) Zhong, W.; Vanderbilt, D.; Rabe, K. *Phys. Rev. B* **1995**, *52*, 6301-6312.

(34) Geneste, G.; Dammak, H.; Thiercelin, M.; Hayoun, M. *Phys. Rev. B* **2013**, *87*, 014113.

(35) Azad, A. M.; Subramaniam, S. *Mat. Res. Bull.* **2002**, *37*, 85-97.

(36) Akbarzadeh, A. R.; Kornev, I.; Malibert, C.; Bellaiche, L.; Kiat, J. M. *Phys. Rev. B* **2005**, *72*, 205104.

(37) Kreuer, K. D. *Annu. Rev. Mater. Res.* **2003**, *33*, 333-359.

(38) In *Proton Conductors: Solids, membranes and gels - materials and devices*; Colomban, P., Ed.; Campbridge University Press, 1992; Part. V.

(39) Raiteri, P.; Gale, J. D.; Bussi, G. *J. Phys.: Condens. Matter* **2011**, *23*, 334213.

(40) Ottochian, A.; Dezanneau, G.; Gilles, C.; Raiteri, P.; Knight, C.; Gale, J. D. *J. Mater. Chem. A* **2013**, *2*, 3127-3133.

(41) Gonze, X.; *et al.*; *Comput. Phys. Commun.* **2009**, *180*, 2582-2615.

(42) Geneste, G.; Torrent, M.; Bottin, F.; Loubeyre, P.; *Phys. Rev. Lett.* **2012**, *109*, 155303.

(43) Rossi, M.; Ceriotti, M.; Manolopoulos, D. E. *J. Chem. Phys.* **2014**, *140*, 234116.

[12]

[12]J. Chem. Theory Comput. 12, (2016) 1351-1359. DOI: 10.1021/acs.jctc.5b01146

Graphical TOC Entry